Structural, optical and electrical properties of WO_xN_y films deposited by reactive dual magnetron sputtering

Sodky H. Mohamed[1,2] and André Anders[1]

[1]Lawrence Berkeley National Laboratory, 1 Cyclotron Road, California 94720, USA

[2]Physics Department, Faculty of Science, South Valley University, 82524 Sohag, Egypt

Abstract

Thin films of tungsten oxynitride were prepared by dual magnetron sputtering of tungsten using argon/oxygen/nitrogen gas mixtures with various nitrogen/oxygen ratios. The presence of even small amounts of oxygen had a great effect not only on the composition but on the structure of WO_xN_y films, as shown by Rutherford backscattering and x-ray diffraction, respectively. Significant incorporation of nitrogen occurred only when the nitrogen partial pressure exceeded 89% of the total reactive gas pressure. Sharp changes in the stoichiometry, deposition rate, room temperature resistivity, electrical activation energy and optical band gap were observed when the nitrogen/oxygen ratio was high. The deposition rate increased from 0.31 to 0.89 nm/s, the room temperature resistivity decreased from 1.65×10^8 to 1.82×10^{-2} Ωcm, the electrical activation energy decreased from 0.97 to 0.067 eV, and the optical band gap decreased from 3.19 to 2.94 eV upon nitrogen incorporation into the films. WO_xN_y films were highly transparent as long as the nitrogen

incorporation was low, and were brownish (absorbing) and partially reflecting as nitrogen incorporation became significant.

Keywords: Dual magnetron sputtering; tungsten oxynitride thin films; structural, electrical, optical properties

1. Introduction

Tungsten trioxide (WO_3) has a high capability to reversibly change its optical properties by insertion or extraction of small (e.g. H, Li) ions and charge-compensating electrons [1]. This makes it suitable for use in a variety of applications such as smart windows, nonemissive display devices, variable reflectance mirrors, and variable emissivity surfaces [1, 2]. WO_3 is also used as an active layer in gas sensors since it has the ability to decrease its high resistance when gasses are adsorbed [3, 4]. Tungsten nitrides, on the other hand, are characterized by high melting point, high hardness, chemical inertness and good thermal stability [5]. For these reasons, they are used for diffusion barriers in microelectronics [6, 7] and electrodes in semiconductor devices [8]. Therefore, a combination of these materials as tungsten oxynitride, WO_xN_y, promises the possibility to tune the structural, optical and electrical properties in a wide range as desired for various applications.

In the last decade, transition metal oxynitride thin films have received considerable interest due to their interesting properties. The introduction of nitrogen into the oxide lattice or oxygen into the nitride lattice resulted in modifications of the film properties. For example, the substitution of oxygen by nitrogen in the TiO_2 [9], ZrO_2 [10] or Ta_2O_5 [11] lattice increased the index of refraction. This is because the metal-nitrogen bonds tend to be less polar than the corresponding metal-oxygen bonds, which leads to a higher polarizability for the metal nitrides [12] and a decrease of the optical band gap. The color is particularly changed by the more covalent bond character introduced by nitrogen upon oxygen replacement in A-WO_x, where A is a rare earth element [13], or by nitrogen replacement in ZrN [14]. The introduction of oxygen into the tungsten nitride lattice relieves residual stress [15]. Transition metal oxynitrides can be used in numerous applications; for example, CrO_xN_y can be used for temperature–dependence resistors in thermal radiation detectors [16], TiO_xN_y can serve as diffusion barriers in silicon-on-sapphire integrated circuits [17] and as decorative coatings [18], HfO_xN_y can be used as gate material in metal-oxide-semiconductor devices [19], and rare earth-WO_xN_y materials are promising as novel pigments [13]

Reactive dual magnetron sputtering is a well established process for the deposition of compound films. The term “dual” refers to the presence of two magnetrons whose targets serve as alternating cathode and anode. The material is sputtered when the target is

the cathode (negative) and serves as the electron collector when it is the anode (positive). The reasons for using such system are (i) to deal with the "disappearing anode" effect, i.e. the coating of the anode with an insulating film, and (ii) to reduce or prevent arcing on the target. The alternation (switching) of polarity is typically done in the mid-frequency (10-200 kHz) range [20]. In our system, two reactive gases (oxygen, nitrogen) are used which leads to some non-trivial modification of the reactive deposition process [21].

Compared to transition metal oxides and nitrides, the transition metal oxynitrides are poorly explored. In particular, very little has been done on WO_xN_y. The main purpose of this work is to study the compositional, structural, electrical and optical properties of WO_xN_y films as a function of the reactive gas partial pressure ratio.

2. Experimental details

WO_xN_y films were prepared on microscopic glass slides and Si (100) substrates by reactive dual magnetron sputtering of metallic tungsten targets in an argon, oxygen and nitrogen gas mixture. The oxygen-nitrogen gas mixture was feed through a plasma source (of the Constricted Plasma Source type [22] operated at 1500 W. The plasma source was positioned between the two magnetrons. Its purpose was used to enhance the activation of the reactive gases by providing a higher density of ions, excited atoms, and molecules. For

this work, no further studies were done to quantify the effects of the plasma source, as opposed to using reactive gas only.

Sputtering was started with the substrates at room temperature. The substrate was constantly moved, back and forth, in front of the two magnetrons and the plasma source; the closest distance between substrate and targets was 5 cm. An infrared temperature sensor was moving with the substrate recording the temperature of the substrate's backside surface.

The cryogenically pumped vacuum system has a background pressure of 10^{-6} Torr at full pumping speed and about 10^{-5} Torr at the reduced speed used during sputter deposition. The total pressure was kept constant at 40 mTorr monitored by a baratron capacitance manometer. The total pressure was kept constant by adjusting the Ar flow while systematically varying the O_2 and N_2 partial pressures. A differentially pumped gas monitor (PPM 100 by SRS) was used to measure the partial pressures during deposition. This gas monitor was pre-calibrated via readings of the baratron.

To prepare WO_xN_y films, we started with an O_2 partial pressure (P_{O_2}) of 2.74×10^{-3} Torr at 50 sccm O_2 flow. At this oxygen partial pressure, the W targets operate in the "poisoned" mode (oxide layer is present). Next, the O_2 flow was partially replaced by N_2 flow. The N_2 partial pressure (P_{N_2}) increased from 8.35×10^{-5} to 3.93×10^{-3} Torr (corresponding to a flow rate of 0 to 50 sccm N_2) while the O_2 partial pressure decreased

from 2.74×10^{-3} to 2.77×10^{-6} Torr (by reducing the O_2 flow from 50 to 0 sccm). In this way, oxynitride films of different compositions could be obtained. In the remainder of this paper, we will use Γ, which we define as the nitrogen partial pressure normalized by the partial pressures of both reactive gases, $\Gamma \equiv P_{N_2} / \left(P_{N_2} + P_{O_2} \right)$.

The sputtering power was provided by a SPIK pulser (NanoMaster) fed by Pinnacle dual power supply (Advanced Energy). The frequency was set to 50 kHz and the power of 1.5 kW was equally shared between the two magnetrons.

Glass slide substrates were used for x-ray diffraction (XRD) because of the amorphous structure, and for measurements of the optical properties because of the high transparency in the visible range. Si(100) substrates were used for film thickness measurements (Dektak IIA profilometer) and compositional analysis (Rutherford back scattering, RBS). RBS was carried out using a 1.95 MeV $^4He^+$ ion beam generated by a 2.5 MeV Van de Graaff electrostatic accelerator. The samples were mounted on a two-axis goniometer. The backscattered particles were collected by a silicon surface barrier detector positioned at 165° with respect to the incident beam. The samples were tilted at various angles (from 5-50°) to optimize depth resolution. The composition and thickness of the samples were obtained by best fitting the RBS spectra using the standard RUMP analysis software [23].

The crystallographic structure of the films was determined by x-ray diffraction using a Siemens D-500 diffractometer with a Cu tube operated at 40 kV and 30 mA. The measurements were carried out using Cu $K_{\propto}$ radiation with a Ni filter to remove the Cu K_{β} reflections.

The spectral transmittance (*T*) and reflectance (*R*) were measured at normal incidence using a Perkin-Elmer Lambda-19 spectrophotometer in the wavelength range λ=300-2500 nm.

The glass slides had pre-sputtered silver contacts of well defined length and distance, allowing us to record the sheet resistance of the films using a two-terminal configuration. The electrical contacts pads were made by masked silver sputtering, similar to previous work [24]. After film deposition, the samples were placed in an oven and temperature dependent measurements of the dc conductivity were carried out in the range 303 – 503 K. During measurements, the samples were in air and without illumination. A constant voltage of 10 V was applied to the contact pads and the current through the film was measured using a Keithley 410 picoamp-meter.

3. Results and Discussions

3.1 Film composition and structure

Figure 1 shows the deposition rate of WO_xN_y deposited at different partial pressure ratios. The deposition rate was nearly constant up to $\Gamma = 0.693$. A steep increase in deposition rate is observed for $\Gamma > 0.693$. This behavior may be understood by considering the conditions on the target surfaces: a compound layer was formed on the presence of a reactive gas. As long as oxygen was the only reactive gas, the compound layer was tungsten oxide. When nitrogen is introduced and the oxygen partial pressure is reduced, the oxide is partially substituted by a nitride. The fact that the deposition rate was approximately constant up to $\Gamma = 0.693$ indicated that the character of the compound layer had not much changed. For $\Gamma > 0.693$, the compound layer changed; we may conclude that nitrogen reacted with tungsten, at least partially replacing the oxide, leading to a reduction of surface charging and an increase of the sputter yield, among other effects. The higher sputter yield of the nitride can be ascribed to the surface binding energy of the nitride being smaller than that of the oxide. It is interesting to compare this result with the deposition rate of 3 nm/s obtained in a control experiment for the pure metal mode (i.e., Ar gas only). Therefore, going back to our reactive system, the rate of 0.9 nm/s at high Γ indicates that a nitride layer was present on the target and that the system has not yet reached the metal mode.

The composition of WO_xN_y films prepared at different Γ was measured by RBS. The experimental data could be well fitted and interpreted by RUMP simulations. The results are shown in Fig. 2, which indicates that there was no significant nitrogen incorporation for nitrogen partial pressures up to $\Gamma = 0.840$. For $\Gamma > 0.840$, compounds of WO_xN_y were formed. The composition of these films did not linearly dependent on Γ because W possesses a stronger affinity to oxygen than to nitrogen. The oxygen content of the films was always higher than the corresponding nitrogen content in the process gas. Thermodynamically, the formation of tungsten oxide is energetically strongly favored over the formation of tungsten nitride or a NO layer: the heat of formation for WO_3 and WO_2 is -842.9 kJ/mol and -589.7 kJ/mol, respectively, which greatly exceeds the values for W_2N (-22 kJ/mol), WN (-15 kJ/mol) [25], and NO (91.3 kJ/mol) [26, 27]. Furthermore, from Fig. 2 one can see that even if some of the nitrogen atoms were adsorbed and "buried" by the arriving W atoms [9], they did not become incorporated for $\Gamma \leq 0.840$. This may be ascribed to a nitrogen desorption mechanism which is induced by oxygen reacting with the W-[NO]-W structure, where nitrogen is released from the network as an interstitial NO molecule, leaving a peroxy linkage in its place [28].

Figure 3 shows typical XRD patterns of WO_xN_y films deposited at different Γ. The pure WO_3 film is amorphous (Fig. 3a); the broad peak centered at about $2\theta = 25°$ stems

from the glass substrate. This was expected since WO_3 crystallizes only when the temperature exceeds 200°C [29], while the maximum temperature that the film could reach via the plasma process heating was about 170°C. No change in the amorphous structure was observed as long as Γ did not exceed 0.993. The observed peaks for the films prepared at $\Gamma = 0.999$ can be associated with cubic WN [30]. It is interesting to note that the transition from amorphous to crystalline structures does not exactly coincide with the start of nitrogen incorporation. Nitrogen incorporation was observed for $\Gamma > 0.889$, whereas crystalline phases were observed for $\Gamma > 0.992$. The formation of a specific crystalline phase is affected by the composition, the temperature, and the possibility of competitive growth of different phases. In the WO_xN_y system, it is also possible that WO_xN_y crystallize in a single phase and that a nanocomposite multiphase structure may form [31] containing substoichiometric WO_x and WN_y as well as stoichiometeric WO_3 and WN crystallites. It is further noticed that the stoichiometry for $\Gamma = 0.999$ films was $WN_{1.8}$, determined by RBS, which contains more nitrogen than the stoichiometric WN. The excess nitrogen atoms are believed to exist at the grain boundaries between tungsten nitride crystallites [32].

3.2 Electrical Properties

Tungsten oxide, WO_3, is a wide band n-type semiconductor that is very insulating as long as the material is stoichiometric, whereas tungsten nitride has metallic character. Figure 4 shows the room temperature resistivity of WO_xN_y films as a function of Γ. The resistivity of WO_3 films deposited at $\Gamma = 0.029$ was 1.65×10^8 Ωcm. This value is higher than the reported values (10^3-10^7 Ωcm) for r. f. sputtered WO_3 films [33] It is known that the conductivity of WO_3 films depends on the O_2/Ar ratio during the sputtering process [33]. According to Gillet *et al.* [34] the conductivity of WO_3 is governed by the non-stoichiometry which originates from oxygen vacancies. The high resistivity value stayed almost constant upon increasing Γ to 0.840. For $\Gamma > 0.840$, the resistivity decreased sharply to reach a value of 1.8×10^{-2} Ωcm at $\Gamma = 0.999$. This can be explained by the increase of the metallic bond contribution and the formation of nitrogen doped WO_3, as was proposed for zirconium oxynitride [14].

The electrical conductivity σ can be written as an exponential function of temperature, *T*,

$$\sigma(T) = \sigma_0 \exp(-E_A / k_B T)\,, \qquad (1)$$

where E_A is the activation energy for electrical conduction, which is a function of the electronic energy levels of the chemically interacting atoms in the amorphous materials and hence of the emerging band gap, σ_0 is the pre-exponential factor including the charge

carrier mobility and density of states, and k_B is the Boltzmann constant. The activation energy can be derived from an Arrhenius plot of such dependence (Fig. 5), and the results for various films obtained at different Γ are compiled in Fig. 6. The activation energy and pre-exponential factor show sharp decrease upon nitrogen incorporation in the WO_3 films. Electronic conduction takes place in the extended state above the mobility edge or by hopping in localized states that can be distinguished on the basis of the pre-exponential factor, σ_0. It was suggested by Mott and Davis [35] (p. 382) that the pre-exponential factor for conduction in localized states should be two or three orders smaller in magnitude than for conduction in the extended states and should become still smaller for conduction in the localized states near the Fermi level. If the value of the pre-exponential factor is in the range of 10^3–10^4 Ω^{-1}cm^{-1}, the conduction is mostly in extended states. A smaller value of the pre-exponential factor would indicate a wide range of localized states and conduction by hopping [36] In our WO_xN_y thin films, the calculated σ_0 values for the films prepared for $\Gamma < 0.889$ are in the range of 10^6 Ω^{-1}cm^{-1}. This suggested that the conduction in these films is due to thermally assisted charge carrier movement in the extended states. The calculated σ_0 values for the films prepared at $\Gamma > 0.889$ are in the range of 10^1 - 10^2 Ω^{-1}cm^{-1}. Therefore, the possibility of extended state conduction is decreased and localized states conduction in the band tail is most likely. The incorporation of nitrogen in the film

modified the microstructure and induced states near the conduction band thereby increasing the carrier density.

3.3 Optical Properties

Figure 7 shows the optical transmittance spectra of WO_xN_y films deposited at various Γ. There was no significant change in transmittance upon increasing Γ up to 0.840. For $\Gamma > 0.840$, the absorption edge shifted towards greater wavelengths. The films changed from colorless for $\Gamma \leq 0.840$ to light brownish for $0.840 < \Gamma < 0.993$. For $\Gamma > 0.993$, metallic WO_xN_y films with higher absorption were obtained.

Using the measured spectral transmittance and reflectance, and the film thickness, *d*, the absorption coefficient α was calculated according to

$$\alpha = \frac{1}{d} \ln\left(\frac{1-R}{T}\right). \quad (2)$$

The optical band gap, E_g, was experimentally determined using Tauc's formula[37]

$$\alpha h\nu = \beta(h\nu - E_g)^n \quad (3)$$

where β is a constant and *n* is equal to 2 or ½ for allowed indirect or direct transitions, respectively. The E_g values are extracted from the $(\alpha h\nu)^{1/2}$ vs. $h\nu$ plot, indicating an indirect band gap for all of the examined WO_xN_y films. The band gap E_g shows a sharp decrease upon nitrogen incorporation in WO_3 film (Fig. 8). Band gap narrowing by

nitrogen incorporation has been previously observed in different transition metal oxynitrides [9, 10, 12, 15, 16].

Different approaches have been adopted to interpret this effect. Investigations by Futsuhara *et al.* [38] provided an interpretation based on the change in ionicity upon nitrogen incorporation. The optical band gap was related to the difference in ionicity between metal-O and metal-N bonds. Ionicity in a single bond increases with the difference in values of electronegativity between two elements forming the bond. The electronegativity of oxygen (3.5) is greater than that of nitrogen (3.0), which indicates that the metal-O bond involves a larger charge transfer than the metal-N bond. Thus, assuming that metal-O and metal-N bonds coexist in the films, the shift of the band gap can be attributed to the decrease in ionicity and hence to an increase of polarizability as the nitrogen content is increased.

A different approach based on density of states calculations was introduced by Asahi *et al.* [39]. They concluded that the substitutional doping of N into TiO_2 leads to the band gap narrowing by mixing N 2*p* states with O 2*p* states. This second approach is supported by simulations by Choi *et al.* [40] who investigated the HfO_xN_y system. They demonstrated that the N 2*p* states extends toward the conduction band as the N concentration increases and the ionic character of Hf-N bonding is less pronounced, resulting in a reduction of the band gap.

4. Conclusions

Tungsten oxynitride films were prepared by reactive dual magnetron sputtering on glass and Si(100) substrates at different oxygen and nitrogen partial pressures. Nitrogen is only incorporated in the films at relatively high partial pressures of nitrogen. As nitrogen is incorporated, interesting modifications of the stoichiometric, structural, electrical and optical properties occur due to new electronic states which reduce the band gap and resistivity, and change the mechanism of conduction. With increasing nitrogen content, the films changes from highly transparent to brownish semi-reflecting. These oxynitride films may be used for decorative coatings and they are also interesting for electronic devices such as sensors in thermal radiation detectors.

Acknowledgements

The authors are grateful for technical support by Sakon Sansongsiri and Michael Dickinson. One of us (S. H. M.) would like to express his sincere gratitude to the Fulbright Commission for a fellowship to carry out this research work at Lawrence Berkeley National Laboratory. This work was also supported by the Assistant Secretary for Energy Efficiency and Renewable Energy, Office of Building Technology, of the U.S. Department of Energy under Contract No. DE-AC02-05CH11231.

References

[1] C. G. Granqvist, *Handbook of Inorganic Electrochromic Materials*. Amsterdam: Elsevier, 1995.

[2] C. G. Granqvist, E. Avendano, and A. Azens, *Thin Solid Films* 442 (2003) 201.

[3] M. Stankova, X. Vilanova, E. Llobet, J. Calderer, C. Bittencourt, J. J. Pireaux, and X. Correig, *Sensors and Actuators B* 105 (2005) 271.

[4] J. Guérin, K. Aguir, M. Bendahan, and C. Lambert-Mauriat, *Sensors and Actuators B* 104 (2005) 289.

[5] L. E. Toth, *Transition Metal Carbides and Nitrides*. New York: Academic Press, 1971.

[6] B. H. Lee and K. Yong, *J. Vac. Sci. Technol. B* 22 (2004) 2375.

[7] J. S. Becker and R. G. Gordon, *Appl. Phys. Lett.* 82 (2003) 2239.

[8] B.-L. Park, M.-B. Lee, K.-J. Moon, H.-D. Lee, H.-K. Kang, and M.-Y. Lee, "Comparison of PECVD-WN_x and CVD-TiN films for the upper electrode of Ta_2O_5 capacitors," IEEE 1998 Int. Interconnect Technol. Conf., San Francisco, CA, 1998, 96-98.

[9] S. H. Mohamed, O. Kappertz, J. M. Ngaruiya, T. Niemeier, R. Drese, R. Detemple, M. M. Wakkad, and M. Wuttig, *physica status solidi (a)* 201 (2004) 90.

[10] J. M. Ngaruiya, O. Kappertz, C. Liesch, P. Müller, R. Dronskowski, and M. Wuttig, *physica status solidi (a)* 201 (2004) 967.

[11] S. Venkataraj, D. Severin, S. H. Mohamed, J. Ngaruiya, O. Kappertz, and M. Wuttig, *Thin Solid Films* 502 (2006) 228.

[12] M. Ohring, *Materials Science of Thin Films. Deposition and Structure*, 2nd ed. San Diego: Academic Press, 2002.

[13] N. Diot, O. Larcher, R. Marchand, J. Y. Kempf, and P. Macaudiere, *J. Alloys and Compounds* 323-324 (2001) 45.

[14] P. Carvalho, F. Vaz, L. Rebouta, L. Cunha, C. J. Tavares, C. Moura, E. Alves, A. Cavaleiro, P. Goudeau, E. L. Bourhis, J. P. Riviere, J. F. Pierson, and O. Banakh, *J. Appl. Phys.* 98 (2005) 023715.

[15] Y. G. Shen and Y. W. Mai, *J. Mater. Res.* 15 (2000) 2437.

[16] R. Mientus, R. Grötschel, and K. Ellmer, *Surf. Coat. Technol.* 200 (2005) 341.

[17] N. Kumar, M. G. Fissel, K. Pourrezaei, B. Lee, and E. C. Douglas, *Thin Solid Films* 153 (1987) 287.

[18] F. Vaz, P. Cerqueira, L. Rebouta, S. M. C. Nascimento, E. Alves, P. Goudeau, J. P. Riviere, K. Pischow, and J. de Rijk, *Thin Solid Films* 447-448 (2004) 449.

[19] C.-L. Cheng, K.-S. Chang-Liao, and T.-K. Wang, *Solid-State Electronics* 50 (2006) 103.

[20] E. V. Barnat and T.-M. Lu, *Pulsed Sputtering and Pulsed Bias Sputtering*. Boston: Kluwer Academic Publishers, 2003.

[21] W. D. Sproul, D. J. Christie, and D. C. Carter, *Thin Solid Films* 491 (2005) 1.

[22] A. Anders, R. A. MacGill, and M. Rubin, *IEEE Trans. Plasma Sci.* 27 (1999) 82.

[23] L. R. Doolittle, *Nucl. Instrum. Meth. Phys. Res. B* 9 (1985) 344.

[24] E. Byon, T. H. Oates, and A. Anders, *Appl. Phys. Lett.* 82 (2003) 1634.

[25] F. R. de Boer, R. Boom, W. C. M. Mattens, A. R. Miedema, and A. K. Niessen, *Cohesion of Metals*. Amsterdam: North Holland, 1988.

[26] (Ed.), *Handbook of Chemistry and Physics, 81st Edition*. Boca Raton, New York: CRC Press, 2000.

[27] M. Uekubo, T. Oku, K. Nii, M. Murakami, K. Takahiro, S. Yamaguchi, T. Nakano, and T. Ohta, *Thin Solid Films* 286 (1996) 170.

[28] W. Orellana, A. J. R. da Silva, and A. Fazzio, *Phys. Rev. B* 72 (2005) 205316.

[29] E. Washizu, A. Yamamoto, Y. Abe, M. Kawamura, and K. Sasaki, *Solid State Ionics* 165 (2003) 175.

[30] *Powder Diffraction Files, Joint Committee on Powder Diffraction Standards, JCPDS, Card 65-2898.*, 1998.

[31] O. Banakh, T. Heulin, P. E. Schmid, H. L. Dreo, I. Tkalcec, F. Levy, and P. A. Steinmann, *J. Vac. Sci. Technol. A* 24 (2006) 328.

[32] M. H. Tsai, S. C. Sun, H. T. Chiu, and S. H. Chuang, *Applied Physics Letters* 68 (1996)

1412.

[33] S. C. Moulzolf, S.-a. Ding, and R. J. Lad, *Sensors and Actuators B* 77 (2001) 375.

[34] M. Gillet, C. Lemire, E. Gillet, and K. Aguir, *Surface Science* 532-535 (2003) 519.

[35] N. F. Mott and E. A. Davis, *Electronics Processes in Non-Crystalline Materials*. Oxford: Clarendon, 1979.

[36] S. A. Khan, M. Zulfequar, Z. H. Khan, M. Ilyas, and M. Husain, *Optical Materials* 20 (2002) 189.

[37] J. Tauc, *Amorphous and Liquid Semiconductors*. New York: Plenum Press, 1974.

[38] M. Futsuhara, K. Yoshioka, and O. Takai, *Thin Solid Films* 317 (1998) 322.

[39] R. Asahi, T. Morikawa, T. Ohwaki, K. Aoki, and Y. Taga, *Science* 293 (2001) 269.

[40] J. Choi, R. Puthenkovilakam, and J. P. Chang, *Ext. Abstr. Electrochem. Soc.* 502 (2006) 522.

Figure Captions

Fig. 1 Deposition rate of WO_xN_y as a function of the normalized nitrogen partical pressure,

$\Gamma = P_{N_2} \big/ \left(P_{N_2} + P_{O_2} \right)$.

Fig. 2 Oxygen and nitrogen concentrations in WO_xN_y films as a function of

$\Gamma = P_{N_2} \big/ \left(P_{N_2} + P_{O_2} \right)$.

Fig. 3 X-ray diffraction patterns of WO_xN_y deposited at different Γ.

Fig. 4 Room temperature resistivity of WO_xN_y films as a function of Γ.

Fig. 5 Arrhenius plot of the conductivity, ln(σ) versus 1000/T, σ in Ω cm, for WO_xN_y films prepared at various $\Gamma = P_{N_2} \big/ \left(P_{N_2} + P_{O_2} \right)$.

Fig. 6 Electrical activation energy (a), and the pre-exponential factor (b), calculated from the slopes and the intercepts of Fig. 5, respectively, as a function of $\Gamma = P_{N_2} \big/ \left(P_{N_2} + P_{O_2} \right)$.

Fig. 7 Transmittance of WO_xN_y films prepared at various $\Gamma = P_{N_2} \big/ \left(P_{N_2} + P_{O_2} \right)$. The thicknesses of the films were in the range 420-600 nm.

Fig.8 Optical band gap of WO_xN_y films as a function of $\Gamma = P_{N_2} \big/ \left(P_{N_2} + P_{O_2} \right)$.

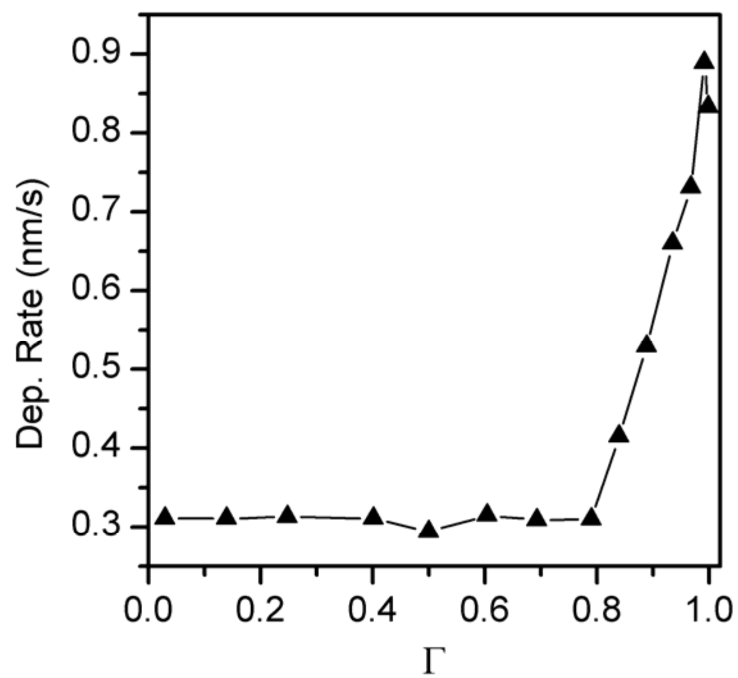

Fig. 1

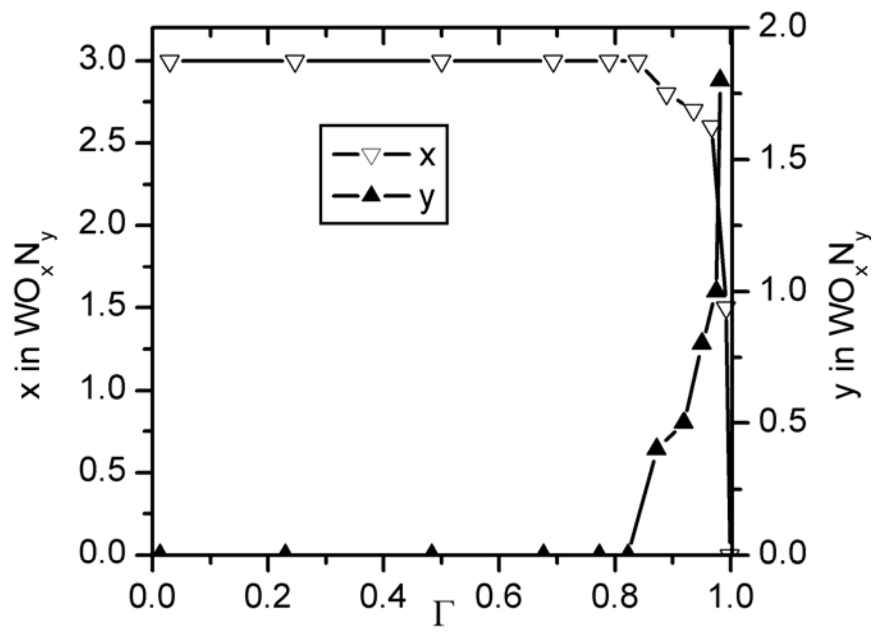

Fig. 2

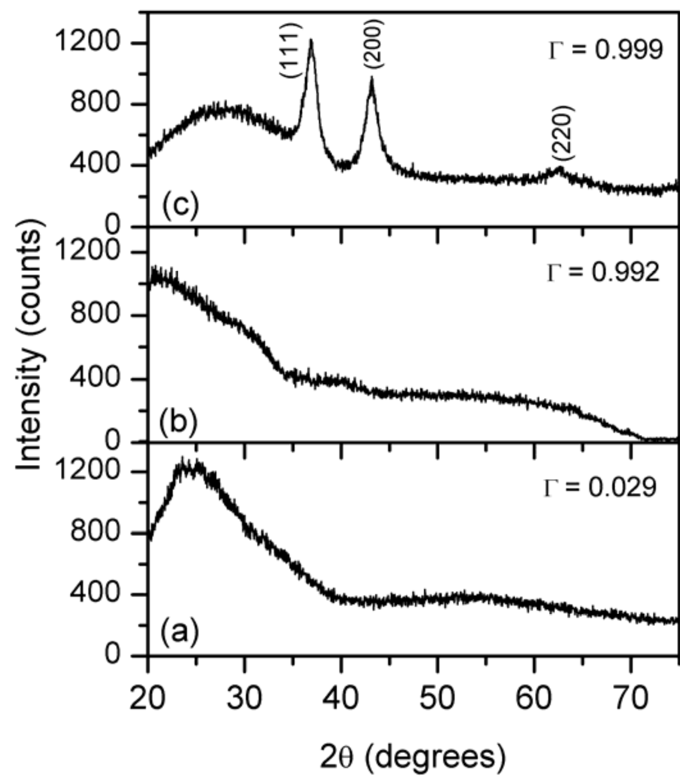

Fig. 3

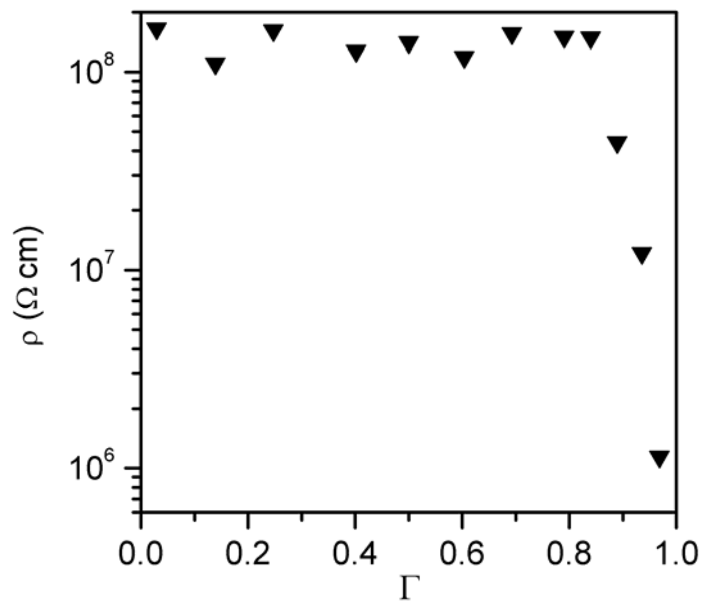

Fig. 4

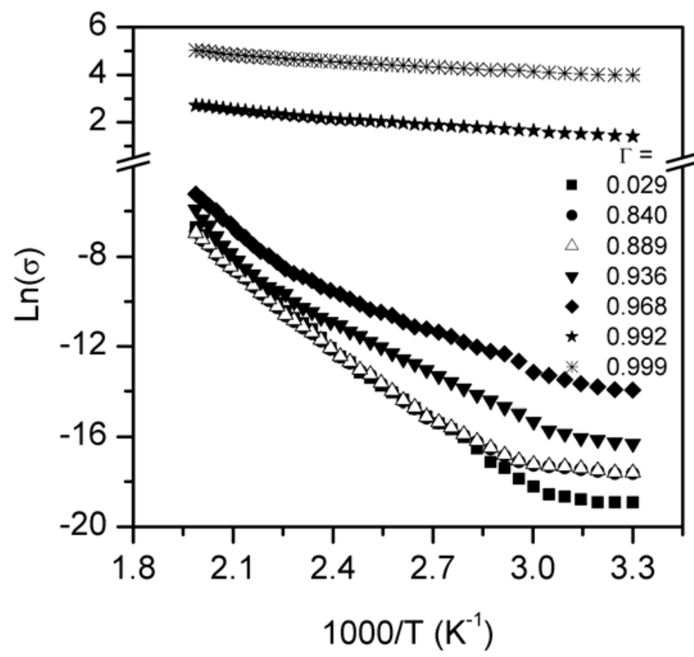

Fig. 5

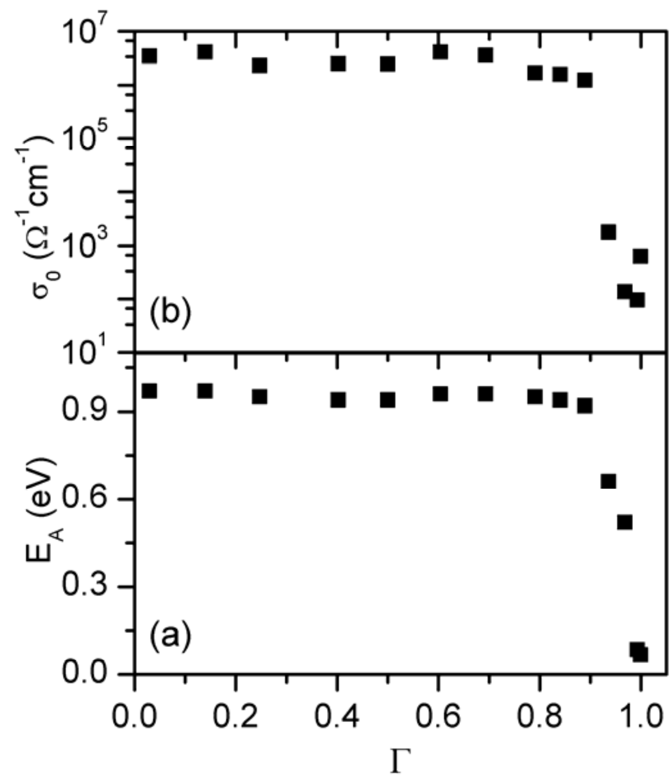

Fig. 6

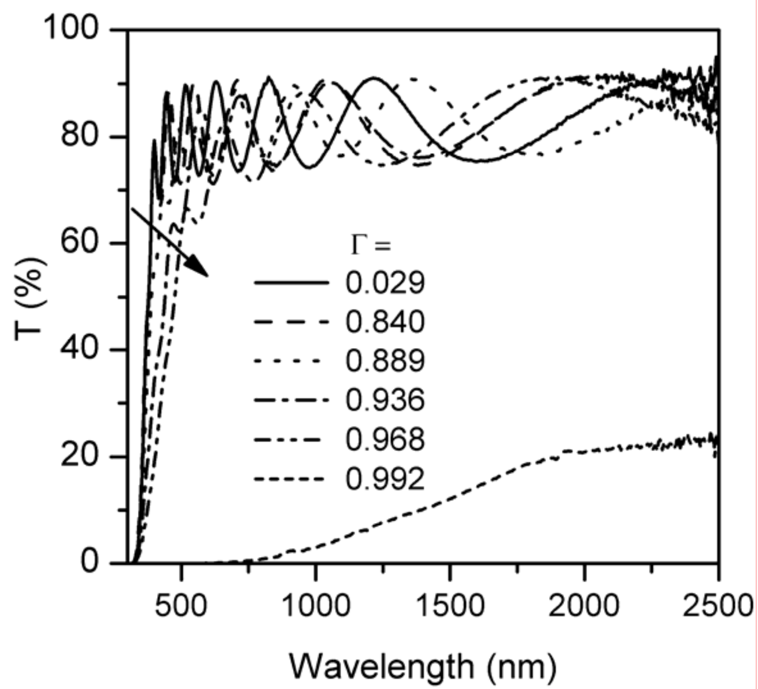

Fig. 7

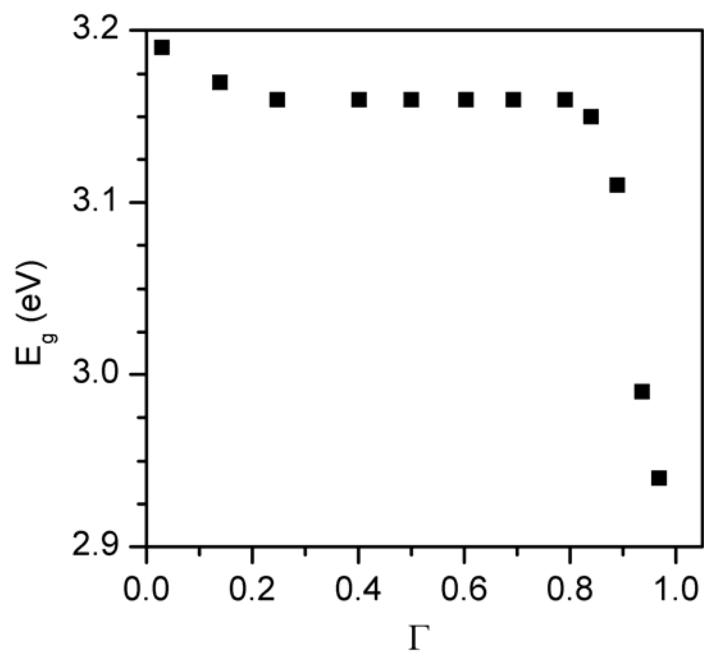

Fig. 8